Subsalt Marchenko imaging: A Gulf of Mexico example

Xueyi Jia, Antoine Guitton, Satyan Singh, and Roel Snieder

ABSTRACT

Marchenko redatuming allows one to use surface seismic reflection data to generate the seismic response at any point in the subsurface due to sources at the surface. Without requiring much information about the earth's properties, the seismic response generated by Marchenko redatuming contains accurate estimates of not only the primaries, but also internal multiples. A target-oriented imaging method, referred to as Marchenko imaging, was implemented for imaging complex structures of the earth using the seismic response obtained through Marchenko redatuming. Taking account of the contribution of both primaries and internal multiples, Marchenko imaging provides more accurate information about the earth's structures than standard imaging methods (e.g. Reverse Time Migration). In order to apply Marchenko redatuming and imaging to field seismic data, we investigate two important aspects of the Marchenko framework: 1) the missing near offsets in marine shot records, and 2) the calibration of the reflection data. With numerical experiments using a Gulf of Mexico salt model (inspired by a Gulf of Mexico field dataset), we present a criterion to determine whether the missing near offsets of the towed-streamer dataset need to be reconstructed. We also demonstrate the importance of proper calibration for the amplitudes of the reflection data in removing the artifacts caused by the mismatch between the amplitudes of the two inputs, the reflection response and the first arrival, for Marchenko redatuming. Finally, we suggest a work flow for processing the marine towed-streamer field dataset acquired at the Gulf of Mexico, and present a complete theoretical and practical framework to produce a target-oriented subsalt image using the Marchenko methods. The images obtained from Marchenko imaging are consistent and comparable, for the most part, with conventional migration methods. However, Marchenko imaging achieves improvements in the continuity of the geological structures and in suppressing the artifacts, which we think are caused by internal multiples.

1 INTRODUCTION

Marchenko imaging is a technique to image the subsurface of the earth using both the primaries and multiples of seismic data, and aims to produce an image that is free of artifacts caused by multiple reflections. This imaging approach is based on the redatumed reflection response created by a method referred to as Marchenko redatuming, which virtually moves the surface seismic sources and receivers to a deeper depth, close to the targets in the medium. Significantly, the redatumed data contain only the reflection response below the redatuming depth, and the medium above is treated as reflection-free. Therefore, Marchenko imaging provides a target-oriented solution specifically for imaging the area below complex structures such as salt bodies (which can create strong multiples).

Marchenko redatuming (the core of the Marchenko frame work) contains two steps: receiver redatuming and source redatuming (Figure 1). Receiver redatuming, also referred to as autofocusing, aims to retrieve wavefields from sources at the surface to a virtual receiver in the medium using Marchenko-type equations. Classic redatuming methods (Berryhill, 1979, 1984; Kinneging et al., 1989) do not account for internal multiple reflections; hence, spurious events can emerge when there is only single-sided illumination (Snieder et al., 2006). With Marchenko redatuming, both the primaries and the multiples can be correctly estimated (Rose, 2002; Broggini et al., 2012; Wapenaar et al., 2014b), and the retrieved wavefields are naturally separated into up- and downgoing components. In the second step of source redatuming, these up- and downgoing wavefields can be utilized to move the sources to the redatuming level by approaches such as multidimensional deconvolution (van der Neut et al., 2011). Unlike the wavefield retrieval method that uses seismic interferometry, which requires the data recorded at a physical receiver in the subsurface(Bakulin and Calvert, 2006), Marchenko redatuming requires only surface seismic data and a background velocity model as inputs, which are the same requirements for many standard imaging techniques (e.g. Reverse Time Migration). A background velocity model is used to compute the traveltime of the first arrival from a subsurface point to the surface, instead of being used to perform any wavefield propagation. In general, the Marchenko redatuming process does not require any more details of the medium parameters than conventional imaging schemes (Broggini et al., 2014).

Broggini and Snieder (2012) first show the scheme to

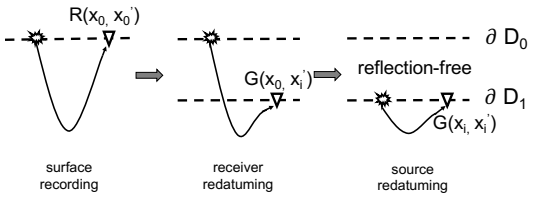

Figure 1. Illustration of the source and receiver levels for surface recording, after receiver redatuming and after source redatuming.

use Marchenko equations to retrieve the Green's functions between an arbitrary virtual source position inside the 1D medium and a receiver at the surface with only the reflection response recorded at the surface of that medium. Wapenaar et al. (2014a,b) then derive the 3D Marchenko equations, which relate the single-sided reflection response of a 3D medium to a focusing wavefield, of which the focusing point is defined by estimating the traveltime from this point to the surface.

Marchenko redatuming has been extended to elastic media by using P- and S- wave measured potentials from P- and S- wave potential sources (Wapenaar, 2014) and by using velocity-stress recordings from force and deformation sources (da Costa Filho et al., 2014). Based on the latter approach, an elastic Marchenko imaging method has been proposed (da Costa Filho et al., 2015). All of the above redatuming methods are under the assumption that surface-related multiples are eliminated in the data. Singh et al. (2015) show that free surface multiples can be directly handled by adding an extra integral that represents the free surface effect in the Marchenko equations (Singh et al., 2015), thus bypassing the need to apply surface-related multiple elimination (SRME) to the data.

For field data applications, target-oriented Marchenko imaging has been applied to an ocean-bottom cable (OBC) survey recorded over the Volve North Sea field (Ravasi et al., 2016), and an adaptive Marchenko imaging scheme has been applied to a marine streamer dataset (Van Der Neut et al., 2015). The application to the Volve field dataset presents some encouraging results, as the image produced by Marchenko imaging is more continuous compared to a standard RTM image. Moreover, Marchenko imaging reveals some structural features that are not present in the surface RTM image. However, the geological structures are relatively simple in both examples.

In this paper, we demonstrate a successful application of Marchenko redatuming and imaging to a marine streamer dataset acquired over a salt structure at the Gulf of Mexico. With a salt body, this dataset provides sufficient complexities to test the Marchenko redatuming and imaging methods. In a standard marine towed-streamer survey, the near-offset data cannot be recorded, and the data contain only one-sided offsets. Hence, we first perform a set of synthetic experiments to investigate whether the data acquired with such geometry satisfy the requirement for the reflection response of Marchenko redatuming. Finally we present a work flow (starting from the processing of the raw field data) to produce a subsalt Marchenko image. We review each step in the working flow: processing the raw data, estimating the direct arrival, redatuming through Marchenko iteration scheme, and imaging using deconvolution imaging condition. Finally, we analyze the subsalt Marchenko image and compare it to a standard RTM image created with the same dataset, and discuss the improvements gained in the Marchenko image.

2 METHODOLOGY

In this section, we outline the methodology for the Marchenko framework, including receiver redatuming, source redatuming, and imaging. We focus on the implementation and physical interpretation of receiver redatuming, and briefly discuss the source redatuming and imaging algorithms used in our application. Readers who do not want the details of the mathematical derivations for receiver redatuming, can treat the Marchenko redatuming process as a black box. Given a background velocity model and the surface seismic reflection response, the black box accurately produces the seismic wavefield recorded at a pre-defined subsurface point (responding to the surface sources) with both primary and multiple reflections. In other words, the black box retrieves a virtual reverse Vertical Seismic Profile (rVSP) as if a virtual receivers was placed inside the medium, and recorded data due to sources at the surface. Moreover, the retrieved wavefield is decomposed into two components: the upgoing component, which contains the energy that is propagating upward when it arrives at the virtual receiver, and the downgoing component, which contains the energy that is propagating downward when it arrives the virtual receiver.

2.1 Receiver redatuming (autofocusing)

In this study, we use a iterative scheme for receiver redatuming which is adapted from the work of Broggini et al. (2014) on the basis of the earlier theoretical Marchenko frameworks (Rose, 2002; Broggini et al., 2012; Wapenaar et al., 2014b). The heart of the Marchenko redatuming is the reciprocity theorem. The convolution- and correlation-type reciprocity theorems relate two wave states with different field, material, and source properties in heterogeneous media (de Hoop, 1988; Wapenaar et al., 2004; Vasconcelos et al., 2009). Source-receiver reciprocity, which states that the same waveform will be observed if the locations of the source and receiver are exchanged, is a special case of the reciprocity theorem.

Figure 2 shows the two wave states we choose to relate by the reciprocity theorem in order to derive the Marchenko-type equations. State A is represented by the focusing functions (upgoing component f^- and downgoing component f^+) which are defined in a modified medium that is reflection-free below the focusing level ∂D_i. State B is represented by the actual wavefields in the subsurface (upgoing component G^- and downgoing component G^+). In the following discussion, we refer to these physical wavefields as the up- and downgoing

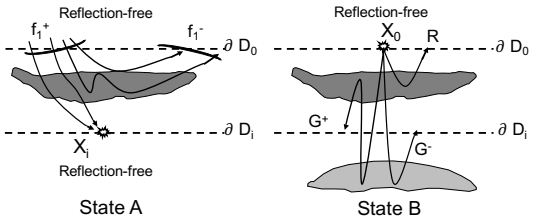

Figure 2. Illustration of the two wavefield states considered in Marchenko redatuming.

Green's functions because the wavefields of state B represent the responses to impulsive point sources. In all our examples, the "Green's functions" shown in the figures are convolved with a Ricker wavelet for display purposes.

According to the one-way reciprocity theorem, the Green's functions and the focusing functions are related by (Wapenaar et al., 2014b; Neut et al., 2014)

$$G^-(x_i,x_0,\omega) = -f_1^-(x_0,x_i,\omega) + \int_{\partial D_0} R(x_0,x_0^{'},\omega) f_1^+(x_0^{'},x_i,\omega) dx_0^{'}; \quad (1)$$

$$G^+(x_i,x_0,\omega) = [f_1^+(x_0,x_i,\omega)]^* - \int_{\partial D_0} R(x_0,x_0^{'},\omega)[f_1^-(x_0^{'},x_i,\omega)]^* dx_0^{'}. \quad (2)$$

Here $G^-(x_i,x_0,\omega)$ and $G^+(x_i,x_0,\omega)$ are the frequency-space domain up- and downgoing Green's functions, with a point source at x_0 at the acquisition surface and a receiver at x_i at a desired subsurface location. The focusing functions $f_1^-(x_0^{'},x_i,\omega)$ and $f_1^+(x_0^{'},x_i,\omega)$ are the up- and downgoing parts of the solution for a specified wave equation whose wavefield focuses at the subsurface location x_i. $R(x_0,x_0^{'},\omega)$ contain the earth's reflection response to a vertical dipole source at $x_0^{'}$ (recorded by a pressure receiver at x_0). The left multiplication is equivalent to convolution in the time-space domain, while * denotes complex conjugation.

We solve for $G^-(x_i,x_0,\omega)$ and $G^+(x_i,x_0,\omega)$ by decomposing equations 2 into two time windows: t ¡ t_d and t ¿ t_d, where t_d is the direct arrival travel time from the focusing point x_i to the surface. In the time window when $t < t_d$, the Green's functions $G^+(x_0,x_i,\omega)$ and $G^-(x_0,x_i,\omega)$ are equal to zero. We first decompose f^+ into a direct wave T_d^{inv} and a following coda M^+:

$$f_1^+(x_0,x_i,\omega) = T_d^{inv}(x_0,x_i,\omega) + M^+(x_0,x_i,\omega), \quad (3)$$

and then substitute $f_1^+(x_0,x_i,\omega)$ in equations 2 with equation 3. Next, we compute the focusing functions by the following iterative scheme in the time window $t < t_d$:

$$[M_k^+(x_0,x_i,\omega)]^* = \int_{\partial D_0} R(x_0,x_0^{'},\omega)[f_{1,k}^-(x_0^{'},x_i,\omega)]^* dx_0^{'};$$
$$f_{1,k+1}^-(x_0,x_i,\omega) = \int_{\partial D_0} R(x_0,x_0^{'},\omega) M_k^+(x_0^{'},x_i,\omega) dx_0^{'} + f_{1,0}^-(x_0,x_i,\omega), \quad (4)$$

with the initial value of f_1^- computed by

$$f_{1,0}^-(x_0,x_i,\omega) = \int_{\partial D_0} R(x_0,x_0^{'},\omega) T_d^{inv}(x_0^{'},x_i,\omega) dx_0^{'}; \quad (5)$$

where T_d^{inv} is the time-reversal of the direct arrival from the focusing point to surface T_d^{inv}. Note that T_d^{inv} is also the initial value of f_1^+, and T_d^{inv} can be computed with any approach that can calculate travel time between two points with a given background velocity model.

Finally, in the time window when $t < t_d$, $G^-(x_i,x_0,\omega)$ and $G^+(x_i,x_0,\omega)$ are obtained by substituting the $f_1^-(x_0^{'},x_i,\omega)$ and $f_1^+(x_0^{'},x_i,\omega)$ into equations 2.

2.2 Source redatuming

Once the up- and down-going Green's functions are correctly retrieved, we use them to obtain the redatumed reflection response $\tilde{R}(x_i,x_i^{'},\omega)$ that satisfies (Wapenaar et al., 2014b),

$$G^+(x_0,x_i,\omega) = \int_{\partial D_i} \tilde{R}(x_i,x_i^{'},\omega) G^-(x_0,x_i^{'},\omega) dx_i^{'} \quad (6)$$

Here $\tilde{R}(x_i,x_i^{'},\omega)$ can be interpreted as the redatumed reflection response as if both the sources and receivers are placed at depth level ∂D_i in a medium that is identical to the physical medium below ∂D_i and homogeneous above (as shown in the right part of Figure 1). Such redatumed data only contain the seismic reflection events resulting from the geological structures below ∂D_i. Significantly, any complex overburden between the acquisition depth ∂D_0 and redatumed depth ∂D_i (e.g. weather layers or salt bodies) does not affect the redatumed data. In this study, we use the multidimensional deconvolution (MDD) approach proposed by van der Neut et al. (2011) and Wapenaar et al. (2014b) to solve equation 6 and obtain $\tilde{R}(x_i,x_i^{'},\omega)$.

2.3 Imaging

The redatumed reflection response $\tilde{R}(x_i,x_i^{'},\omega)$ can be used in different ways for imaging. One approach is to obtain the full reflection response by redatuming the sources and receivers at the same depth level, and then utilize the redatumed data to form a seismic image below the redatuming depth level using any established imaging algorithms (e.g. RTM). Note that a velocity model for the areas below the redatuming depth level is needed if one wants to perform RTM using the redatumed data in this way.

An alternative approach for imaging (what we use) is

more straightforward: for every image point inside a target zone, we extract the zero-offset and zero-time component $\tilde{R}(x_i, x_i, t = 0)$ from the redatumed reflection response $\tilde{R}(x_i, x_i^{'}, t)$, and construct an image of the zero-offset reflectivity using

$$I(x_i) = \tilde{R}(x_i, x_i, t = 0). \quad (7)$$

With this imaging condition, we can compute the reflectivity of every image point in a target zone. Significantly, the image produced in both ways is free of spurious reflections, as $\tilde{R}(x_i, x_i^{'}, t)$ contain accurate information for both the primary and multiple wavefields.

3 SYNTHETIC EXAMPLES

We first demonstrate and interpret the up- and downgoing Green's function retrieved by Marchenko receiver redatuming with a synthetic example for a subsurface point in a 2D acoustic medium (which contains a salt body). We verify the retrieved Green's function by comparing it with the Green's function for the same subsurface point which is obtained through directly modeling using the finite difference method. Next we investigate the influence of the missing near offsets for practical consideration of marine streamer surveys. Finally, we illustrate the importance of calibration for the amplitudes of the data, and discuss how we calibrate the field dataset which we use in the following section.

3.1 Green's function obtained through Marchenko redatuming and finite-difference modeling

As a preparation for our field data application, we demonstrate and interpret the up- and downgoing Green's functions retrieved by Marchenko receiver redatuming with a synthetic example. The background velocity model (Figure 3a) is estimated from a GOM field dataset (the dataset that is used in our field data application). In the corresponding density model (Figures 3a and 3b), we add four flat horizontal reflectors with the thickness of 100 m at the depth levels of 3 km, 4 km, 5 km, and 6 km. The density of these four reflectors are 100 g/cm^3 smaller than the surrounding areas. We generate 1000 shot records with 361 receivers in each shot record using acoustic finite-difference modeling. The spacing between sources and receivers is set as 26.67 m. This synthetic dataset is simulated to match the field dataset for source and receiver locations.

Using Marchenko receiver redatuming, we retrieve the up- and downgoing Green's functions for a subsalt point at $x = 12,225\ m$ and $z = 3,500\ m$, which is referred to as the virtual receiver. The retrieved downgoing Green's function (Figure 4a) can be interpreted as the seismic wavefields that are excited by the surface sources and are propagating downward when they reach the virtual receiver. The first event (labeled with a) in the downgoing Green's function is the direct arrival from the surface sources to the virtual receiver. The downgoing Green's function contains internal multiples. For

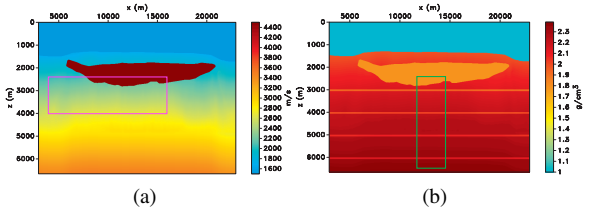

(a) (b)

Figure 3. Illustration of the velocity and density models used for the synthetic examples. (a) Velocity model. Red box encloses the target area for which we produce images using field data. (b) Density model. Green box encloses the target area for which we produce images using synthetic data.

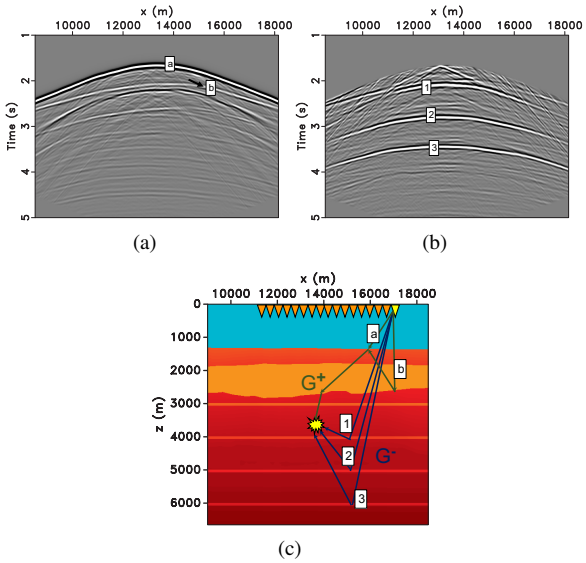

(a) (b)

(c)

Figure 4. (a) Retrieved down-going Green's function G^+. (b) Retrieved up-going Green's function G^-. (c) Physical interpretation of G^+ and G^-.

example, the hyperbola (labeled with b in Figure 4a) corresponds to the internal multiples that are reflected inside the salt body. The ray path of this event is drawn in Figure 4c, also labeled with b. The retrieved upgoing Green's function (Figure 4b) contains the wavefields that are propagating upwards when they reach the virtual receiver. These wavefields start downward propagating from the surface sources and are reflected upward by the structures below the virtual receiver. The three major events in Figure 4b (labeled with 1, 2, and 3) correspond to the primary reflections from the three reflectors below the virtual receiver. Their ray paths are shown in Figure 4c.

The combination of the up- and downgoing Green's functions is the total Green's function recorded at the virtual receiver (Figure 5a). In a numerical experiment to verify the total Green's function retrieved by the Marchenko scheme, we place a line of sources on the surface and a receiver at the same location as the virtual receiver at $x = 13,335m$ and $z = 3,500$ and then record the wavefield directly using finite-

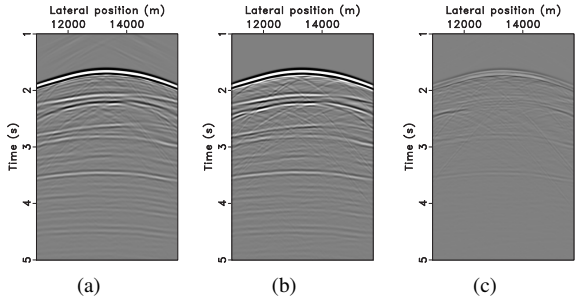

Figure 5. (a) The retrieved the Green's function for a virtual receiver at x=13,335 and z=3,500.The sum of up- and down-going field of Figure 4. (b) The directly modeled Green's function for a virtual receiver at x=13,335 and z=3,500. (c) Difference between the retrieved Green's function in (a) and directly modeled Green's function in (b).

difference modeling. As shown in Figure 5, the wavefield retrieved by the Marchenko redatuming method matches very well with the directly modeled wavefield in the near-offset parts. The retrieved Green's function has some artifacts for far offsets because of the limited acquisition aperture.

3.2 Requirements for acquisition geometry

Marchenko redatuming requires the surface reflection response R to be obtained by an evenly and densely sampled array of sources and receivers with a recording aperture as large as possible. van der Neut et al. (2015) show that the sources and receivers should be placed at the corresponding stationary points to retrieve some particular up- or downgoing events, and sometimes stationary points cover the entire surface. The field dataset used in this study is acquired with the standard towed-streamer acquisition system, which contains traces on only one side of the source for each shot record. One can reconstruct the traces on the other side of each source using the source-receiver reciprocity theorem, forming a dataset with two-sided offsets (given the source line is much longer than the maximum offset). However, the near-offset data cannot be practically acquired for towed marine surveys. In the field dataset we use, offsets from $h = -107m$ to $h = 107m$ (7 traces) are missing. Therefore, we first investigate whether a dataset with missing near offsets in the shot records can be directly used for Marchenko redatuming.

For Marchenko redatuming, each trace in the retrieved Green's functions is constructed by first convolving a trace in the reflection response with a trace in the first arrival, where both traces correspond to the same location at the surface, and then summing over all the source locations (equation 2). In both our synthetic and field examples, there should be 361 traces in each shot record if the near-offsets (including zero offset) can be acquired. With the seven near-offset traces missing in each shot record, each trace in the retrieved Green's functions contains the contribution of the remaining 354 traces. We first consider the moveout time difference Δt between the apex of the hyperbola and the maximum missing near-offset in a shot gather to evaluate the influence of these seven missing traces. Under the conventional assumption that reflection moveout curves are approximated by a hyperbolic equation, Δt is given by

$$\begin{aligned}\Delta t &= \sqrt{t_0^2 + \frac{h^2}{4v_{nmo}^2}} - t_0; \\ &\simeq \frac{h^2}{8v_{nmo}^2 t_0},\end{aligned} \tag{8}$$

where t_0 is the two-way zero-offset travel time, h is the maximum missing near offset, and v_{nmo} is the normal moveout velocity. We are able to obtain a good retrieval of the Green's function from the data with missing near-offsets when the variation of the travel time of the reflection in the missing trace Δt is much less than the dominant wave period T, hence we require that

$$\Delta t \lesssim \frac{T}{8}. \tag{9}$$

Then the maximum missing near offset h should satisfy

$$\begin{aligned}h &\lesssim \sqrt{T v_{nmo}^2 t_0}; \\ &\lesssim \sqrt{2DT v_{nmo}},\end{aligned} \tag{10}$$

where $D = vt_0/2$ is the depth of the first interface of interest. Obviously, with less missing inner traces (smaller h) we obtain a better retrieval of the Green's functions. For the given maximum missing offset h, the larger D, T, and v_{nmo} are, the better the Green's functions are retrieved. In a seismic survey, the dominant wave period can be estimated from the frequency spectrum of the data. Equation 10 tells us that the influence of the missing near offsets becomes smaller for deeper events (larger D and v_{nmo}).

To investigate the influence of the missing near offsets numerically, we generate two synthetic datasets using finite-difference modeling with the velocity and density models used above (Figure 3). The first dataset (a full dataset) contains 361 shot records, with 361 traces in each shot record. For the second dataset (a dataset with missing near offsets), we remove seven receivers near each source (one trace at the some location as the source position and three nearest traces on both sides), and obtain the double-sided dataset with the maximum missing offset of 214 m (identical to the field dataset we use). In this example, D is approximately 15500m, T is 0.1 s, and v_{nmo} is 1500 m/s, so h should be $\lesssim$ 693 m. Since the maximum missing offset (214 m) satisfies the criterion (equation 10), we expect a good retrieval of the Green's functions using the dataset with missing near offsets. Note that the total retrieved Green's functions with the full dataset (Figure 6a) and the dataset with missing near offsets (Figure 6b) are very close to each other. We show the difference panel of these two Green's functions in Figure 6c. The difference panel shows the effect of the missing near-offsets. Some sallow events at the near offset are not fully retrieved using the missing near offset data, which can be predicted by equation 10. In general our approach is not heavily affected by these seven near-offset traces in each shot record.

We perform Marchenko imaging with the method dis-

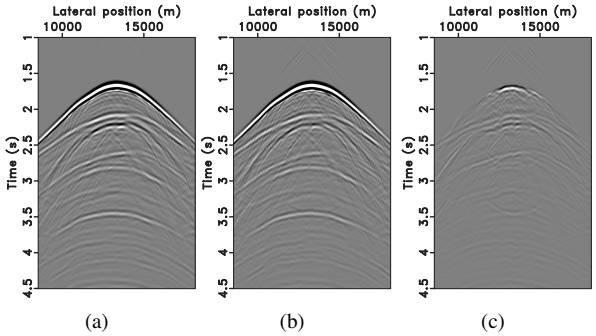

Figure 6. (a) Redatumed field retrieved from the data with full offsets. (b) Redatumed field retrieved from the data with missing near offsets. (c) Difference between (a) and (b).

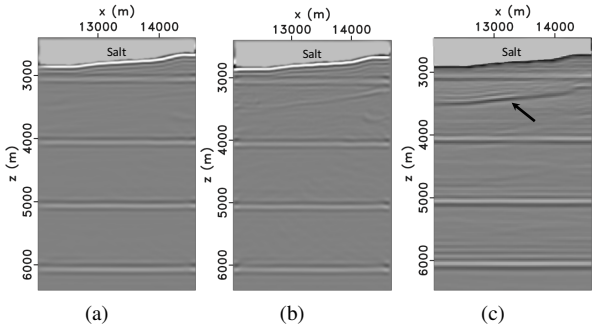

Figure 7. (a) Marchenko image using the data with full offsets. (b) Marchenko image using the data with missing near-offsets. (c) RTM image using the data with full offsets

cussed above for the same target zone (Green box in Figure 3b) using these two datasets and apply reverse time migration (RTM) with the full dataset. According to the density model, the final images should contain the salt bottom and four horizontal reflectors. The Marchenko image produced using the full dataset (Figure 7a) is very similar to the one produced using the dataset with missing near offsets (Figure 7b). Both contain all the expected reflectors. Note that in the RTM image (Figure 7c) an additional reflector appears with a similar shape as the salt bottom. This additional reflector is an artifact introduced by a set of peg-leg internal multiples. This type of artifacts is completely removed in Figure 7a and largely suppressed in Figure 7b.

3.3 Data calibration

The initial step of the iterative scheme in Marchenko redatuming is to convolve the surface reflection response R with the time-reversal of first arrival T_d^{inv} (equation 5). Hence, we need to properly calibrate the amplitudes of R to match the to two inputs, R and T_d^{inv}. We obtain the first arrival from a subsurface point to the surface by: 1) computing the first arriving travel time (using a eikonal solver), and 2) placing a Ricker wavelet at the first arriving travel time. If the maximum amplitude of the Ricker wavelet used is equal to A, the requirement for the surface reflection response R is that R should be the response to a line of impulsive sources with maximum amplitudes equal to $1/A$. The first step to approximate the required R from the surface seismic data D is to estimate the source wavelet and deconvolve the source wavelet from D. We then need to calibrate the deconvolved data obtained from the first step in such way that when we convolve R with T_d^{inv}, the amplitude of the Ricker wavelet A (which is contained in T_d^{inv}) cancels.

In the synthetic examples, we are able to compute the exact scaling factor for data calibration as both the maximum amplitude of the Ricker wavelet A and the source wavelet are known. As shown in Figure 8b. the upgoing Green's function retrieved with the correctly calibrated R is free of artifacts. In Figures 8a and c, we show that the retrieved Green's functions are contaminated with artifacts if the data are not correctly calibrated. Figure 8a shows the upgoing Green's function retrieved using the surface reflection response R which is too small (scaled by a factor of 0.5 relative to the correctly calibrated R). The artifact caused by the incorrect data calibration is depicted in Figures 8a (arrow). When R is too large, the iteration scheme can not converge. In Figure 8c, we show that when the amplitudes of R are too large (where R is multiplied by a scaling factor of 1.5), the retrieved Green's function is dominated by artifacts. We produce three Marchenko images using the Green's functions retrieved from these three sets of surface reflection responses R: the over-calibrated (with a scaling factor equals to 0.5), the correctly-calibrated (with a scaling factor equals to 1), and the under-calibrated (with a scaling factor equals to 1.5). For the over-calibrated case, the artifacts in the Green's functions result in an artifact in the final image (Figures 9a). Note that this artifact shares the shape of the salt bottom and results from an incorrect handling of the internal multiples. For the under-calibrated case, the imaging result completely breaks down (Figures 9c) as the retrieved Green's functions are dominated by artifacts. Finally, in Figures 9b, with the Green's functions retrieved from the correctly calibrated R, we produce an image which is consistent with the velocity and density models and free of artifacts due to multiples.

In the field data application that follows, we obtain the time-reversal of the first arrival T_d^{inv} in a exact same way by using the same velocity model to compute the first arriving time and placing a same Ricker wavelet with a maximum amplitude of A. However, given a surface seismic dataset, we do not have any information about the amplitude of the original source functions. In addition, we do not know what seismic processing steps (e.g. noise attenuation and gain function) the field dataset has gone through, hence the recorded amplitude differs in general from the ture amplitude. Therefore, we calibrate the field dataset by comparing it with the synthetic dataset with missing near offsets (which is used in retrieved the Green's function in Figure 8b). At the same source location, we pick a shot record from the field dataset and a shot record from the synthetic dataset. By dividing the maximum amplitude of each shot record, we obtain the scaling factor for

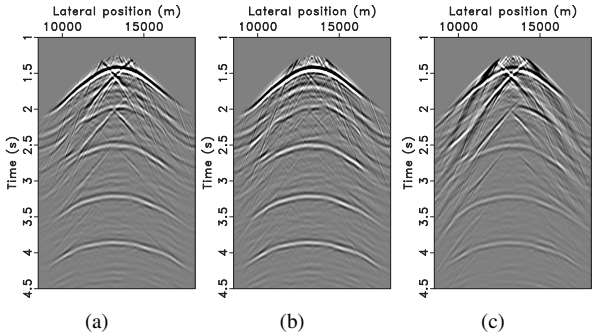

Figure 8. (a) The retrieved upgoing Green's function when the reflection response is scaled by a factor of 0.5. (b) The retrieved upgoing Green's function when the reflection response is scaled by a factor of 1.0. (c) The retrieved upgoing Green's function when the reflection response is scaled by a factor of 1.5.

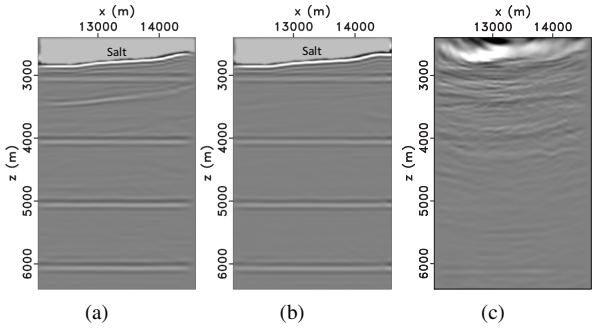

Figure 9. (a) The Marchenko image obtained from the Green's functions retrieved with the reflection response scaled by a factor of 0.5. (b) The Marchenko image obtained from the Green's functions retrieved with the reflection response scaled by a factor of 1.0. (c) The Marchenko image obtained from the Green's functions retrieved with the reflection response scaled by a factor of 1.5.

the calibration of all the field shot records. Note that Ravasi et al. (2016) used a different approach to estimate the scaling factor based on the consideration of the convergence condition of the iterative scheme, and how to properly calibrate a field dataset needs further study.

4 FIELD DATA EXAMPLE: MISSISSIPPI CANYON, GULF OF MEXICO

The 2D marine field dataset we use was acquired over the Mississippi Canyon in the Gulf of Mexico. This area contains a shallow salt body in a deep water environment. A total of 1000 shots were fired along a 26 km source line with a shot spacing of 26.67 m.

4.1 Data Processing

In this study, we design a work flow to apply Marchenko imaging to the streamer dataset (Figure 10). With a background

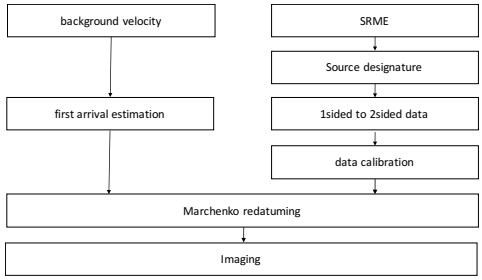

Figure 10. Workflow to apply Marchenko imaging to field data

velocity model, we estimate the direct arrivals from all the subsurface points in the target zone to the surface by computing the travel time using an eikonal solver using fast marching method ((Fomel, 1997)) and placing a Ricker wavelet at the direct arrival time. For the data processing, we 1) apply SRME to the surface seismic data for the suppression of the surface multiples; 2) deconvolve the source signature and the suppress its bubbles; 3) generate the data with two-sided offsets in the common shot gathers based on the data with one-sided offsets; and 4) calibrate the amplitudes of the data using the scaling factor estimated from the comparison with the numerically modeled shot records. Details for data preparation are discussed below.

We start by applying SRME to subtract the surface-related multiple series. Singh et al. (2015) show the approach to retrieve the Green's function in the presence of free-surface multiples. However, in this study, we suppress the free-surface multiples before applying Marchenko redatuming. As shown in equation 4, in the frequency domain implementation of the algorithm, the reflection response $R(\omega)$ is required, not $R(\omega)S(\omega)$ (where the source wavelet is contained in the reflection response). Therefore, the Marchenko redatuming algorithm requires an accurate deconvolution of the source wavelet from the data. We remove the effect of the source signature from the data using the sparse log-domain deconvolution approach of Guitton and Claerbout (2015). Using the reciprocity theorem, we then generate the data with two-sided offsets from the data with one-sided offsets to increase the range of the aperture of the surface reflection response. As discussed above, we do not need to reconstruct the missing near offsets for this dataset. To approximate the physical earth's reflection response R_{real}, after processing the recorded surface data, we also need to calibrate R with a scaling factor s such that $R * s = R_{real}$. Here s is an unknown factor which depends on the acquisition methods and the processing chain. In this application, we find this scaling factor by comparing the maximum amplitude of a field shot record with a synthetic shot record, as we use both the same velocity model and approach to estimate the direct arrivals in both synthetic and field data examples. The amplitudes of the synthetic data match well with the direct arrival; hence, after the data calibration, the amplitudes of the calibrated field data also match with the same direct arrival.

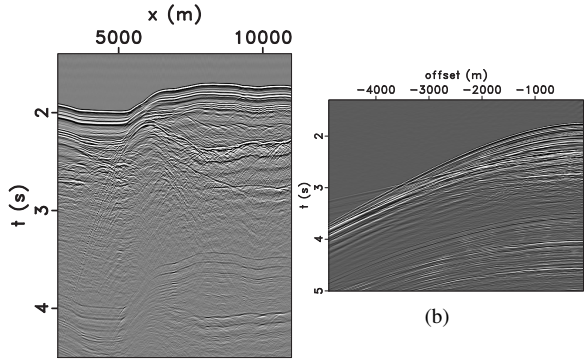

(a) (b)

Figure 11. (a) Raw field data: a near-offset section. (b) Raw field data: a shot record.

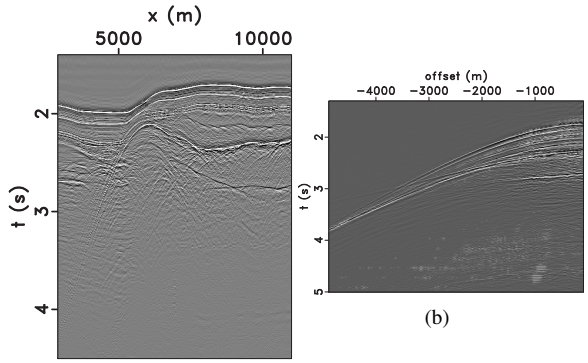

(a) (b)

Figure 12. (a) Field data after source-designature and SRME: a near-offset section. (b) Field data after source-designature and SRME: a shot record.

4.2 Field data Marchenko images

For imaging, we retrieve the up- and downgoing Green's functions for all the subsurface imaging points inside the target zone (red box in Figure 3a, 4.0 km - 16.0 km horizontally and 2.4 km - 4.0 km vertically). This target area contains the bottom and the left edge of the salt body, some sediment layers to the left of the salt body, and structures below the salt body. Following equation 6, we create the redatumed reflection response $\tilde{R}(x_i, x_i^{'}, \omega)$ at each depth level. We then produce the Marchenko image by extracting the zero-time zero-offset value $\tilde{R}(x_i, x_i, t = 0)$, as instructed in equation 7.

A comparison between the Marchenko image (Figure 13b) and the image produced using standard RTM (Figure 13a) shows that they are comparable for the most part: both present similar structures for the bottom of the salt body, the structures of the sediment layers to the left of the salt body, and the detailed structures of the subsalt area. Furthermore, we find significant improvements in the Marchenko image: 1) the reflectors are more continuous and smoother (green arrows in Figures 13a and 13b); 2) the structures of the sediment layers to the left of the salt body are more clearly revealed (red arrows in Figures 13a and 13b); 3) additional structural features are revealed (blue arrows in Figures 13a and Figures 13b).

To better understand these improvements accomplished in the Marchenko image, we produce an RTM image for the same target area using the synthetic dataset generated using the models in Figure 3. In this RTM image (Figure 13c), we observe some artificial reflectors who have a shape similar to the bottom of the salt (dashed green arrow in Figure 13c), which indicates the artifacts result from internal multiple reflections at the salt bottom. When these artificial structures interfere with the horizontal reflector at 3 km, the phases of the horizontal reflector are either added or subtracted, creating amplitude discontinuities (solid green arrows in Figure 13c). Hence, the discontinuities in the field-data RTM image (Figure 13a) could also result from the interference between the multiple artifacts and real sedimentary layers. As the Marchenko imaging method correctly handles internal multiples, it is able to produce an image (Figure 13b) that is more continuous and free from the multiple artifacts. The layered structures to the left of the salt body (red arrows in Figures 13a and 13b), revealed both in the RTM image and the Marchenko image, are sedimentary layers beneath the seabed. Note that the amplitudes of these sedimentary layers in the RTM image are suppressed, while the layers are more clearly revealed and more comprehensible in the Marchenko image (red arrows in Figure 13a and 13b). Moreover, Marchenko imaging reveals some structural features (blue arrows in Figure 13b) that are not presented in the RTM image.

5 CONCLUSIONS AND DISCUSSION

For the first time, we successfully apply subsalt Marchenko redatuming and imaging to a marine dataset from the Gulf of Mexico. With some numerical experiments, we investigate the effect of the missing near-offset traces, and conclude that the artifacts caused by multiples can be largely supressed by directly using the missing near offset data. We show that calibration of the data need to be properly performed, and we calibrate the data based on the comparison with the numerically modeled dataset in this study.

We present that the image produced by Marchenko imaging is more continuous than the RTM image produced using the same dataset and velocity model. Furthermore, the Marchenko method seems able to reveal some structures that cannot be found in the RTM image. We use an RTM image produced with a synthetic dataset to demonstrate that the discontinuities in the RTM image are very likely caused by internal multiples. The improvements in the Marchenko image over the RTM image demonstrate that for field data, the Marchenko frame work is applicable and effective in suppressing the artifacts caused by internal multiples.

6 ACKNOWLEDGMENTS

We thank sponsors of the Center for Wave Phenomena, whose support made this research possible. The reproducible nu-

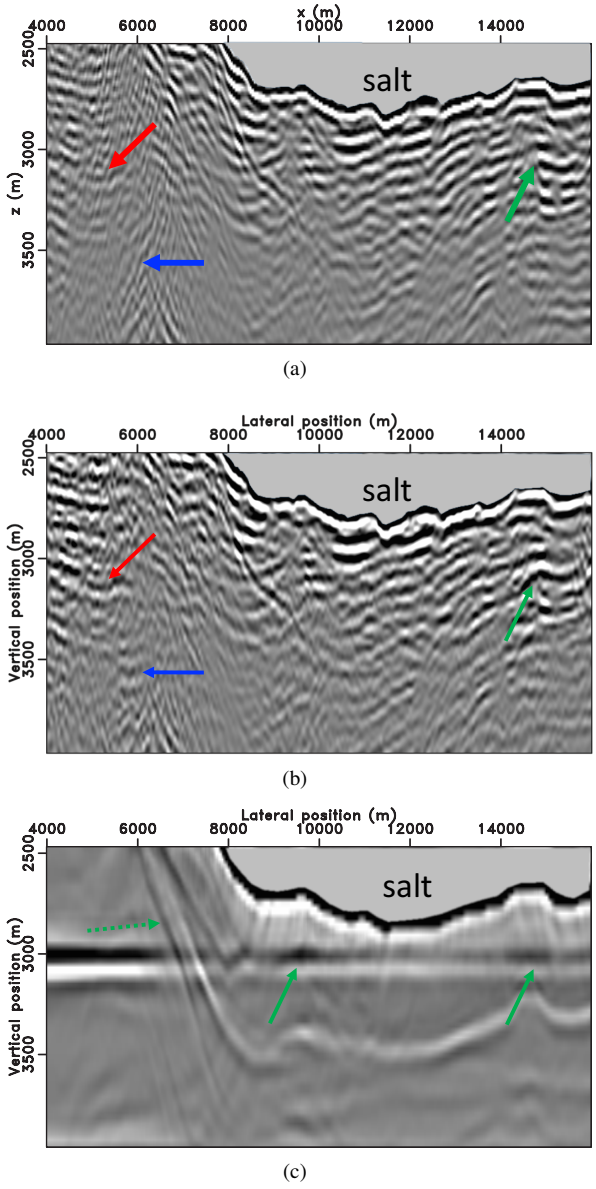

Figure 13. (a) RTM image with the field dataset. (b) Marchenko image with the field dataset. (c) RTM image with the synthetic dataset generated from velocity and density models in Figure 3.

meric examples in this paper use the Madagascar open-source software package (Fomel et al., 2013) freely available from http://www.ahay.org. We are grateful to D. Witters for her help in reviewing this manuscript and F. Broggini, C. and A. da Costa Filho for discussions.

REFERENCES

Bakulin, A., and R. Calvert, 2006, The virtual source method: Theory and case study: Geophysics, **71**, SI139–SI150.

Berryhill, J. R., 1979, Wave equation datuming: GEOPHYSICS, **44**, 1329–1344.

———, 1984, Wave equation datuming before stack: GEOPHYSICS, **49**, 2064–2066.

Broggini, F., and R. Snieder, 2012, Connection of scattering principles: a visual and mathematical tour: Eur. J. Phys., **33**, 593–613.

Broggini, F., R. Snieder, and K. Wapenaar, 2012, Focusing the wavefield inside an unknown 1d medium: Beyond seismic interferometry: Geophysics, **77**, A25–A28.

———, 2014, Data-driven wavefield focusing and imaging with multidimensional deconvolution: Numerical examples for reflection data with internal multiples: Geophysics, **79**, WA107–WA115.

da Costa Filho, C. A., M. Ravasi, and A. Curtis, 2015, Elastic p-and s-wave autofocus imaging with primaries and internal multiples: Geophysics, **80**, S187–S202.

da Costa Filho, C. A., M. Ravasi, A. Curtis, and G. A. Meles, 2014, Elastodynamic green's function retrieval through single-sided marchenko inverse scattering: Physical Review E, **90**, 063201.

de Hoop, A. T., 1988, Time-domain reciprocity theorems for acoustic wave fields in fluids with relaxation: The Journal of the Acoustical Society of America, **84**, 1877–1878.

Fomel, S., 1997, A variational formulation of the fast marching eikonal solver: SEP-95: Stanford Exploration Project, 127–147.

Guitton, A., and J. Claerbout, 2015, Nonminimum phase deconvolution in the log domain: A sparse inversion approach: Geophysics, **80**, WD11–WD18.

Kinneging, N., V. Budejicky, C. Wapenaar, and A. Berkhout, 1989, Efficient 2d and 3d shot record redatuming1: Geophysical Prospecting, **37**, 493–530.

Neut, J. v. d., K. Wapenaar, J. Thorbecke, and I. Vasconcelos, 2014, Internal multiple suppression by adaptive marchenko redatuming, *in* SEG Technical Program Expanded Abstracts 2014: Society of Exploration Geophysicists, 4055–4059.

Ravasi, M., I. Vasconcelos, A. Kritski, A. Curtis, C. A. d. C. Filho, and G. A. Meles, 2016, Target-oriented Marchenko imaging of a North Sea field: Geophysical Journal International, **205**, 99–104.

Rose, J. H., 2002, Single-sided autofocusing of sound in layered materials: Inverse Problems, **18**, 1923–1934.

Singh, S., R. Snieder, J. Behura, J. van der Neut, K. Wapenaar, and E. Slob, 2015, Marchenko imaging: Imaging with primaries, internal multiples, and free-surface multiples: Geophysics, **80**, S165–S174.

Snieder, R., K. Wapenaar, and K. Larner, 2006, Spurious multiples in seismic interferometry of primaries: Geophysics, **71**, SI111–SI124.

van der Neut, J., J. Thorbecke, K. Mehta, E. Slob, and K. Wapenaar, 2011, Controlled-source interferometric redatuming by crosscorrelation and multidimensional deconvolution in elastic media: Geophysics, **76**, SA63–SA76.

van der Neut, J., I. Vasconcelos, and K. Wapenaar, 2015, On Green's function retrieval by iterative substitution of the coupled Marchenko equations: Geophysical Journal Inter-

national, **203**, 792–813.

Van Der Neut, J., K. Wapenaar, J. Thorbecke, and E. Slob, 2015, Practical challenges in adaptive marchenko imaging, *in* SEG Technical Program Expanded Abstracts 2015: Society of Exploration Geophysicists, 4505–4509.

Vasconcelos, I., R. Snieder, and H. Douma, 2009, Representation theorems and Green's function retrieval for scattering in acoustic media: Physical Review E, **80**, 036605.

Wapenaar, K., 2014, Single-sided Marchenko focusing of compressional and shear waves: Physical Review E, **90**, 063202.

Wapenaar, K., J. Thorbecke, and D. Draganov, 2004, Relations between reflection and transmission responses of three-dimensional inhomogeneous media: Geophysical Journal International, **156**, 179–194.

Wapenaar, K., J. Thorbecke, J. van der Neut, F. Broggini, E. Slob, and R. Snieder, 2014a, Green's function retrieval from reflection data, in absence of a receiver at the virtual source position.: The Journal of the Acoustical Society of America, **135**, 2847–2861.

———, 2014b, Marchenko imaging: Geophysics, **79**, WA39–WA57.